catalysts

MDPI

Article

Physical and Chemical Synthesis of Au/CeO_2 Nanoparticle Catalysts for Room Temperature CO Oxidation: A Comparative Study

Khaled Mohammad Saoud [1,*] and Mohamed Samy El-Shall [2]

[1] Liberal Arts and Sciences Program, Virginia Commonwealth University in Qatar, Doha, Qatar
[2] Department of Chemistry, Virginia Commonwealth University, Richmond, VA 23284-2006, USA; mselshal@vcu.edu
* Correspondence: s2kmsaou@vcu.edu; Tel.: +974-66037810

Received: 29 October 2020; Accepted: 15 November 2020; Published: 20 November 2020

Abstract: In many heterogeneous catalytic reactions, such as low-temperature CO oxidation, the preparation conditions, and the role of the CeO_2 support (oxygen vacancies and redox properties) in the dispersion and the chemical state of Au, are considered critical factors for obtaining gold nanoparticle catalysts with high catalytic performance. In this work, the physical and chemical preparation methods were compared, aiming at understanding how the preparation method influences the catalytic activity. The Au/CeO_2 nanoparticle catalysts with 5% Au loading were prepared via the Physical Laser Vaporization Controlled Condensation method (LVCC), and the chemical Deposition-Precipitation method (DP) was used to investigate the effect of synthesis methods on the structure and the catalytic activity toward the CO oxidation. In this manuscript, we compare the activity of nanostructured Au/CeO_2 catalysts. The structure and the redox properties of the catalysts were investigated by the XRD, SEM, TEM, TPR, and XPS. The catalytic activity for low-temperature CO oxidation was studied using a custom-built quartz tube flow reactor coupled with an infrared detector system at atmospheric pressure. The study reveals that the prepared CeO_2-supported Au nanoparticles' catalytic activity was highly dependent on the preparation methods. It showed that the sample prepared by the DP method exhibits higher catalytic efficiency toward CO oxidation when compared with the sample prepared by the LVCC method. The high catalytic activity could be attributed to the small particle size and shape, slightly higher Au concentration at the surface, surface-active Au species such as Au^{1+}, along with the large interface between Au and CeO_2. This study suggests that the stability, dispersion of Au nanoparticles on CeO_2, and strong interaction between Au and CeO_2 lead to strong oxidation ability even below room temperature. Considering the universal character of different physical and chemical methods for Au/CeO_2 preparation, this study may also provide a base for supported Au-based catalysts for many oxidation reactions in energy and environmental applications.

Keywords: catalysis; catalyst synthesis; CO oxidation; Au^0; Au^{1+} active site; room temperature CO oxidation; physical preparation; chemical preparation methods; catalyst design

1. Introduction

Metal and metal oxide nanocatalysts, with controlled particle size and high surface area, can significantly improve catalytic performance over conventional catalysts. This research aims at the possibility of designing nanostructured catalysts that possess unique catalytic properties such as low-temperature activity, selectivity, stability, and resistance to poisoning and degradation [1–3]. These catalysts find applications in many fields such as environmental protection, indoor air quality,

and chemical synthesis and processing. Recently, supported precious metals such as platinum, rhodium, and palladium with high activity and stability, even in the presence of moisture and sulfur compounds, have been widely used in CO oxidation and gas exhaust emissions control [4]. Supported gold nanoparticle catalysts have attracted significant attention recently due to their superior catalytic activities in many catalytic reactions [5,6].

In particular, highly dispersed Au nanocatalysts have demonstrated unusual activity toward near-ambient CO oxidation, primarily when supported on reducible metal oxides such as Fe_2O_3, Co_3O_4, CeO_2, and TiO_2 [7–9]. CO oxidation over supported Au catalysts was found to be sensitive to the deposition method of Au, the Au-support interface, the structure/chemical composition of the support, as well as the pre-treatment condition of the catalyst, which is critical in determining the Au nanoparticle morphology and the activity of the Au catalyst [10–12]. Controlling the size and morphology during the synthesis of supported Au nanoparticle catalysts plays an essential role in achieving high surface area, small particle size, and strong metal-support interaction, a factor that influences their catalytic activity toward CO oxidation [13]. Recent studies suggest that the room temperature CO oxidation reaction mechanism over supported Au catalyst is highly dependent on the structure, type of support, and oxidation state of Au, which shape the active site for this reaction. For Au nanocatalysts supported on reducible metal oxides such as TiO_2, the catalytic activity depends on the number of oxygen vacancies at the perimeter interface of the metal oxide surface that play an essential role in molecular oxygen activation [7]. Au particle size also plays a crucial role in the catalytic activity; in this context, the Au nanoparticles supported on CeO_2 were more active than single Au atoms or ions [14]. Theoretical studies suggest that the preparation method of highly active Au catalysts is crucial; for example, the Deposition-Precipitation (DP) method can produce small Au nanoparticles with strong metal support surface interaction, as in the TiO_2 surface, compared to the widely used impregnation method [9,15–18]. All these factors directly influence the design of future highly active catalysts.

Ceria-based supported catalysts play an essential role in three-way catalysts (TWC) by maintaining the catalysts' conversion efficiency [8]. Owing to its superior redox properties, CeO_2 is regarded as one of the best supports in many catalytic systems. CeO_2 can act as oxygen storage by releasing or taking oxygen during oxidation and changing its oxidation state between Ce^{4+}/$Ce3^{+}$ during reduction conditions, making it an essential catalyst for many oxidation reactions [19,20]. CeO_2's unique surface oxygen vacancies enable the coordination and dispersion of Au nanoparticles and enhance the strong synergistic effect between the Au and the CeO_2 support [21]. CeO_2 can store excess oxygen under lean fuel conditions and then release it under fuel-rich conditions according to the following reactions [22]:

$$\text{Rich conditions: } 2CeO_2 + CO \rightarrow Ce_2O_3 + CO_2$$

$$\text{Lean conditions: } Ce_2O_3 + 0.5O_2 \rightarrow 2CeO_2$$

The Au/CeO_2 nanoparticle catalyst has emerged as one of the superior catalysts in recent decades. Recent Temperature Programmed Reduction (TPR) data confirmed that the presence of Au can lead to activation of the ceria and can facilitate the migration of oxygen vacancies from the bulk to the CeO_2 surface [23,24]. Recent studies reported significant enhancement (orders of magnitude) in the catalytic activity of Au/CeO_2 using nanocrystalline CeO_2 (3–5 nm) compared to the conventional catalysts [25]. It has been used in many oxidation reactions, such as low-temperature CO oxidation [22–24,26], water-gas reaction [27,28], and the catalytic combustion of Volatile Organic Compounds (VOC) [29] due to its superior catalytic activity.

The synthesis methods of Au/CeO_2 nanoparticle catalysts with high catalytic activity toward low-temperature CO oxidation could provide a great solution to many environmental issues such as air pollution. Several physical and chemical techniques have been employed in the synthesis of highly active Au/CeO_2 nanoparticle catalysts; most of these processes have employed liquid mixtures or solutions [30–32] or other methods [33]. Recent reports suggest that Au nanoparticles' catalytic

performance is greatly influenced by the size, shape, and chemical and physical properties of supporting materials [34].

Furthermore, the synthesis method can affect the catalytic activity by influencing the Au precursor (metallic or Au cation), as in the case of the classical DP method [35,36], or by changing how Au is introduced onto the support (e.g., chemical methods [37] such as impregnation, precipitation, coprecipitation, and Precipitation-Deposition or physical means such as laser ablation and ion implantation) [8,38,39].

The nature of the Au/CeO_2 nanoparticle catalyst involves many complex factors such as the reduction and interaction of Au with the underlying CeO_2 at the interface and the formation of a reduced nonstoichiometric phase at the interface between them [40,41]. Pre-treatment conditions can also affect the stability of the catalyst, depending on the support nature, thereby increasing the metal-support interaction during the synthesis step and can significantly influence the oxidation state and the nature of the active site of Au-based catalyst. Some studies suggest that Au^0 is the active site [33]. Other studies report Au^{1+} and Au^{3+} species' role in the catalytic activity of the catalyst [42,43]. However, most active samples were obtained without temperature heat treatment (calcination) or via calcination at low temperatures [44,45]. Au nanoparticles can be generated by physical methods where the vapor resulting from the vaporization of bulk Au produce Au atoms in the gas phase, which are later condensed under controlled conditions to form nanoparticles [46]; alternatively, they can be generated by chemical means where Au compounds are used as a starting material, linked with reduction steps.

A few reports focus on the effect of the synthesis method (physical or chemical) on the structure and activity of Au/CeO_2 nanoparticle catalysts, the interaction between CeO_2 and Au, and the redox interplay between Au and CeO_2 during CO oxidation. To investigate this effect on the morphology, shape, and nature of the Au/CeO_2 nanoparticle catalyst's active site, we compared the synthesized Au/CeO_2 using physical (Physical Laser Vaporization Controlled Condensation (LVCC)) and chemical (DP) routes.

2. Results and Discussion

2.1. Characterization of As-Synthesized (Fresh) Au/CeO_2 Nanoparticle Catalyst

2.1.1. Inductive Coupled Plasma (ICP), BET Surface Area, and X-Ray Diffraction (XRD) of As-Synthesized Au/CeO_2 (Fresh) Samples

To confirm the heterogeneity, measure the actual Au loading in both samples, and to ensure anchoring of Au particles on the surface of the CeO_2 support and the sample, inductively coupled plasma-optical emission spectroscopy (ICP-OES) was performed on the synthesized samples. The samples were dissolved in aqua regia and then diluted 20 times. The ICP-OES analysis showed an average Au concentration of ~242.79 ppm (±0.02 ppm) in the Au/CeO_2 (LVCC) sample, which is approximately 4.75 wt% of the catalyst mass, while the Au concentration in the DP sample was 248.86 (±0.02 ppm), which is approximately 4.92 wt%. The ICP results indicate that some Au is leached out during the DP sample synthesis, but both values are close to the 5 wt% Au's theoretical loading.

Owing to the Au nanoparticles' small size, the BET (Brunauer–Emmett–Teller) surface area of the LVCC catalyst was very high at 84.5 m^2/g, compared to the surface area of DP catalyst (23.93 m^2/g).

The X-ray diffraction patterns of the as-synthesized 5% Au/CeO_2 nanoparticle catalyst via the LVCC and DP methods are shown in Figure **??** (compared using the same scale). Although the X-ray diffraction pattern for Au/CeO_2 shows crystalline CeO_2 (JCPDS card no: 34-0394) and (ICCD 00-034-0394) in both catalysts, the two samples exhibited diffraction peaks of the fluorite CeO_2 structure corresponding to CeO_2 (111), CeO_2 (200), CeO_2 (220), CeO_2 (311), CeO_2 (222), CeO_2 (400), and CeO_2 (331) phases, respectively. However, the CeO_2 peaks of the DP sample showed higher intensity than those of the LVCC sample. Furthermore, we compared the full width at half maximum (FWHM) values of CeO_2 (111) for both catalysts and found them to be 0.810 for the LVCC sample and 0.808 for the DP

sample, suggesting the LVCC is broader than the DP peak. Since the Au was not detectable in the fresh DP, and the peak was tiny in the LVCC samples, the FWHM values for Au could not be compared. This result indicates that the DP is more crystalline than the LVCC and that the DP catalyst's particle size is smaller. The BET surface area of the LVCC catalyst was 84.5 m^2/g, compared to the DP catalyst, which had a surface area of 23.93 m^2/g. Surprisingly, the X-ray diffraction patterns of the LVCC sample showed a small broad peak at about 38° (the Au (111) peak assigned to metallic gold). However, no prominent peak related to the Au (111) peak was observed in the DP catalyst, which contradicts the ICP results, which shows a slightly higher Au concentration in the DP sample. These results may be attributed to the dispersion of small Au particles on the support's surface—small-sized Au particles lower than the XRD detection limit (roughly 3 nm) cannot be detected in the XRD [23].

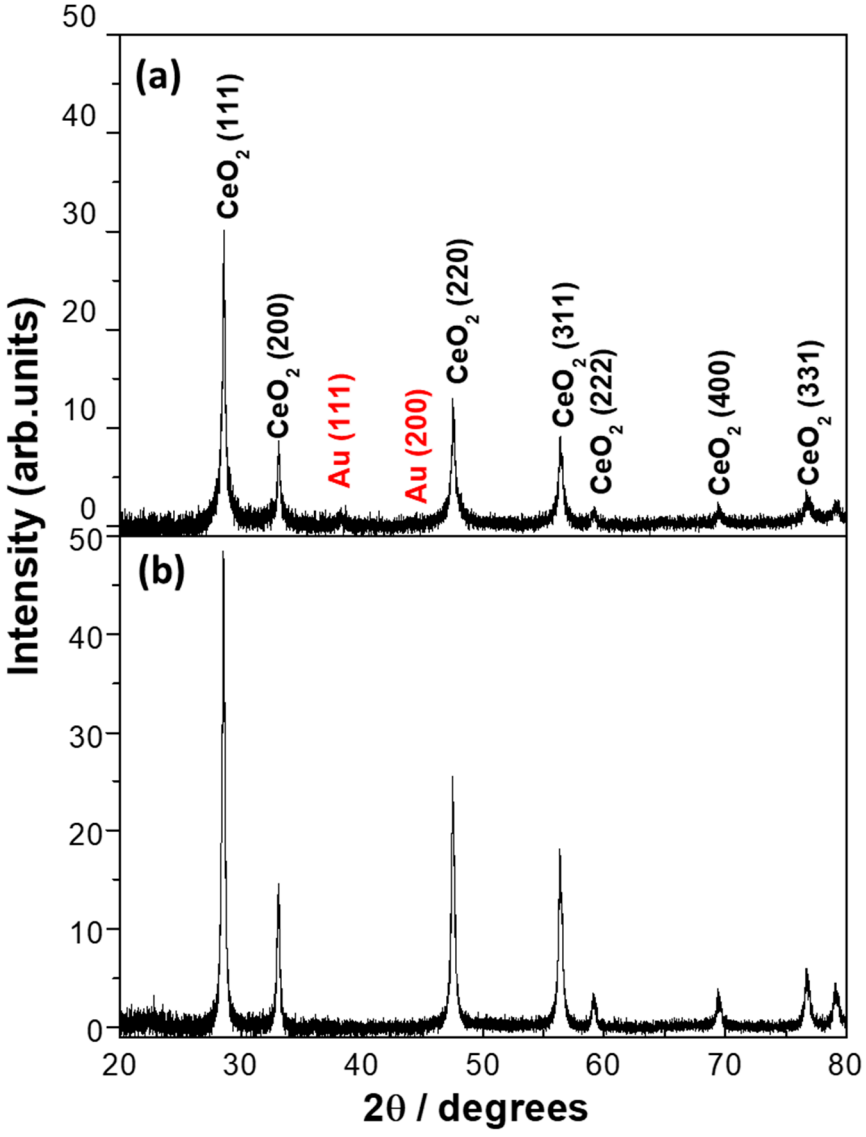

Figure 1. X-ray diffraction patterns of as-synthesized 5% Au/CeO_2 by (**a**) physical method (Physical Laser Vaporization Controlled Condensation (LVCC)) and (**b**) chemical method (Deposition-Precipitation (DP)).

2.1.2. Scanning Electron Microscopy (SEM) of Fresh Au/CeO_2

We performed an SEM on both samples to investigate the catalysts' morphology. Figure 2 shows the SEM micrographs of the LVCC and DP morphologies. Two types of morphologies can be distinguished for the LVCC and DP samples. The LVCC has two types of CeO_2 particles: elongated particles with web-like structures where both Au and CeO_2 are in the nanoscale, and metallic Au nanoparticles

that are dispersed on large CeO_2 spherical particles, as shown in Figure 2a,c. The morphology of DP consists of large aggregates, though the metallic Au nanoparticles cannot be observed on the CeO_2 particles, as shown in Figure 2b,d. Energy Dispersed X-ray (EDX) spectra of fresh wt% Au/CeO_2 nanoparticle catalysts show that both samples consist of Au, Ce, and O_2 with small carbon from the sample holder. However, the LVCC showed a slightly higher amount of Au at the surface of CeO_2 particles (Figure 2a) than the DP sample (Figure 2d).

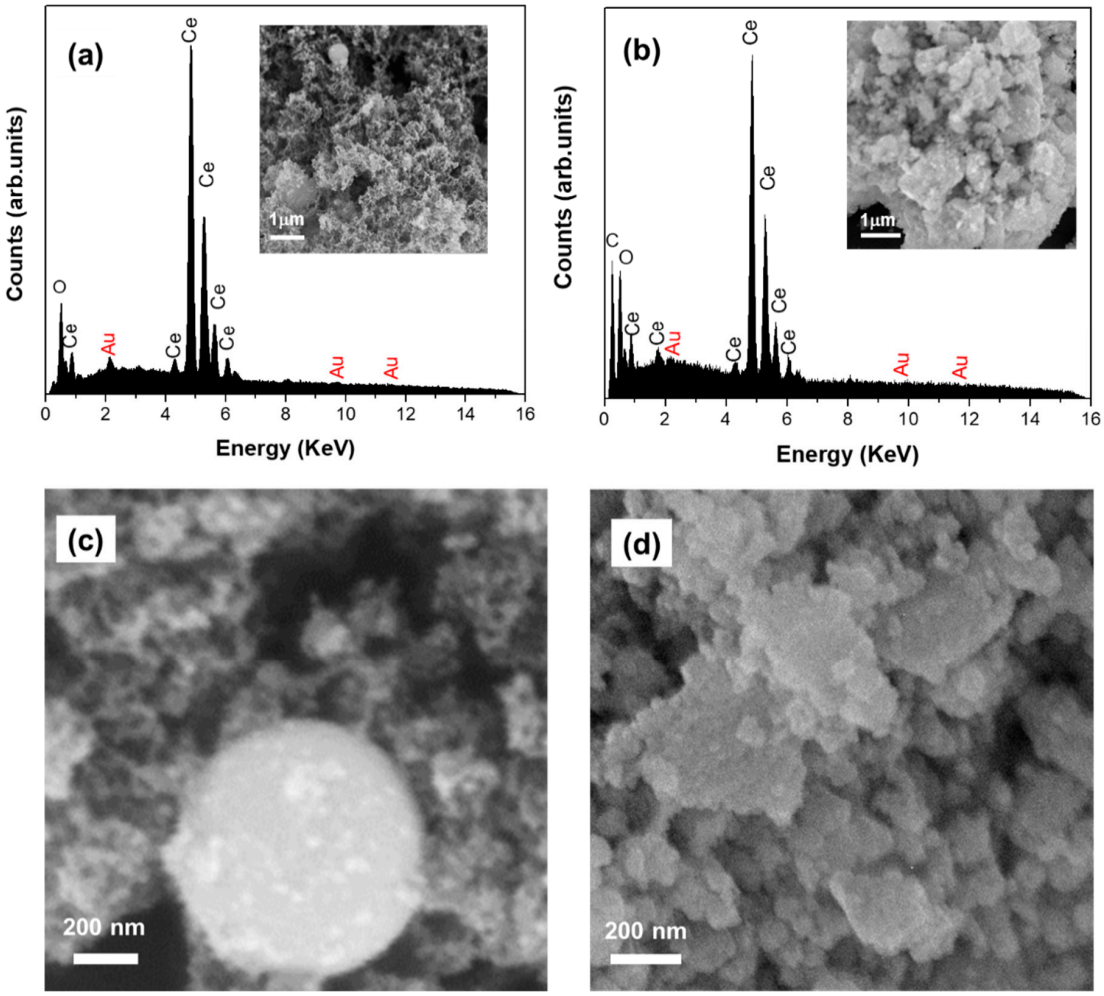

Figure 2. SEM micrographs and Energy Dispersed X-ray (EDX) spectra of fresh 5% Au/CeO_2 nanoparticle catalysts prepared by the physical method (LVCC) (**a**,**c**) and the chemical method (DP) (**b**,**d**).

2.1.3. Transmission Electron Microscopy (TEM) of Fresh Au/CeO_2

The particle size and morphology were further investigated using a Transmission Electron microscope (TEM). Figure 3 shows the morphology and particle size distribution of the fresh Au/CeO_2 catalysts. Figure 3a–c show the TEM micrographs of the fresh LVCC sample; these indicate that the LVCC sample morphology consists of small metallic Au, CeO_2 elongated particles (2–5 nm), and Au particles (5–12 nm) dispersed on large CeO_2 particles (30–500 nm). The Au particles had a broad size distribution of 1–14 nm and an average diameter of 5.4 nm. These results were verified and confirmed via EDX. However, for the DP sample, the phase contrast within the agglomerates was characteristic of disordered, or semi-crystalline, material where the metallic Au nanoparticles had small and narrow size distribution of 1.5–6 nm with an average diameter of 3.4 nm.

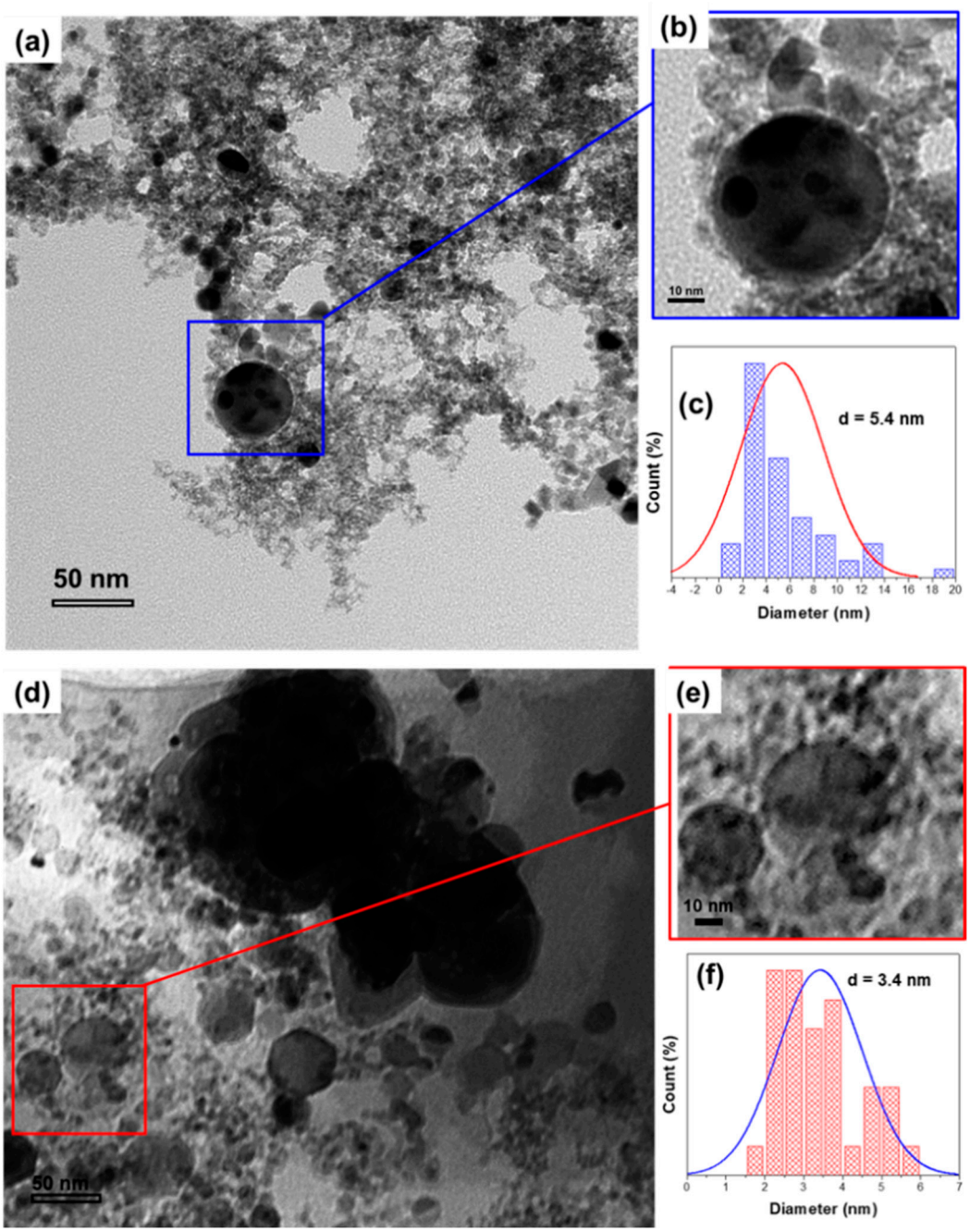

Figure 3. TEM micrographs and particle size distribution of fresh Au/CeO_2 prepared by the physical method (LVCC) (**a**–**c**) and the chemical method (DP) (**d**–**f**).

2.1.4. Chemical and Electronic States: X-Ray Photoelectron Spectroscopy (XPS) of As-Synthesized Au/CeO_2

The XRD and TEM techniques are used to characterize the bulk of the sample and do not provide useful information about the active site for CO oxidation in the catalyst. XRD is not a specific surface technique to obtain information on the nature of surface-active sites. We used X-ray Photoelectron Spectroscopy (XPS) to study the catalyst surface, Au concentration, and determine the oxidation state of Au. XPS was used to probe the active site and investigate the Au species' oxidation states on the catalyst surface of Au/CeO_2.

The XPS results of the analysis of the 5% Au/CeO_2 prepared by LVCC and DP methods are summarized in Table S1. The two powder samples' surfaces contained various amounts of the following

species: cerium as Ce^{4+}, oxygen, carbon as C–(C, H), C–O, C=O, O–C=O, and traces of gold as Au. Figure S2 is a survey scan of all possible elements present in both samples.

The XPS analysis of the Ce 3d and O 1s core-level peaks of LVCC and DP methods is presented in Figure 4. Chemically, the high-resolution Ce 3d spectrum was consistent with Ce^{4+} (including similar shake-up peaks). The spectrum shows two primary peaks, "1" and "4", corresponding to Ce 3d3/2 and Ce 3d5/2 photoelectron peaks. Peaks "2" and "6" are the respective Ce 3d3/2 and Ce 3d5/2 shakedown peaks, while peaks "3" and "5" are the respective Ce 3d3/2 and Ce 3d5/2 shake-up peaks [47]. In the LVCC sample, a tiny peek at ~885.7 eV, as shown in Figure 3a, might indicate the presence of a trace Ce^{3+}, which is reported to have a binding energy of ~885.8 eV, and this peak was not present in the DP sample [48–50]. Furthermore, the peak centered at ~529.7 eV corresponds to O^{2-} or lattice oxygen in CeO_2. Besides, another core-level O 1s peak was observed at the binding energy of 530.24 eV in the LVCC sample, indicating the presence of an oxygen vacancy in the lattice site of CeO_2 nanoparticles [51]. The binding energies of Ce 3d and O 1s are consistent with those of stoichiometric CeO_2.

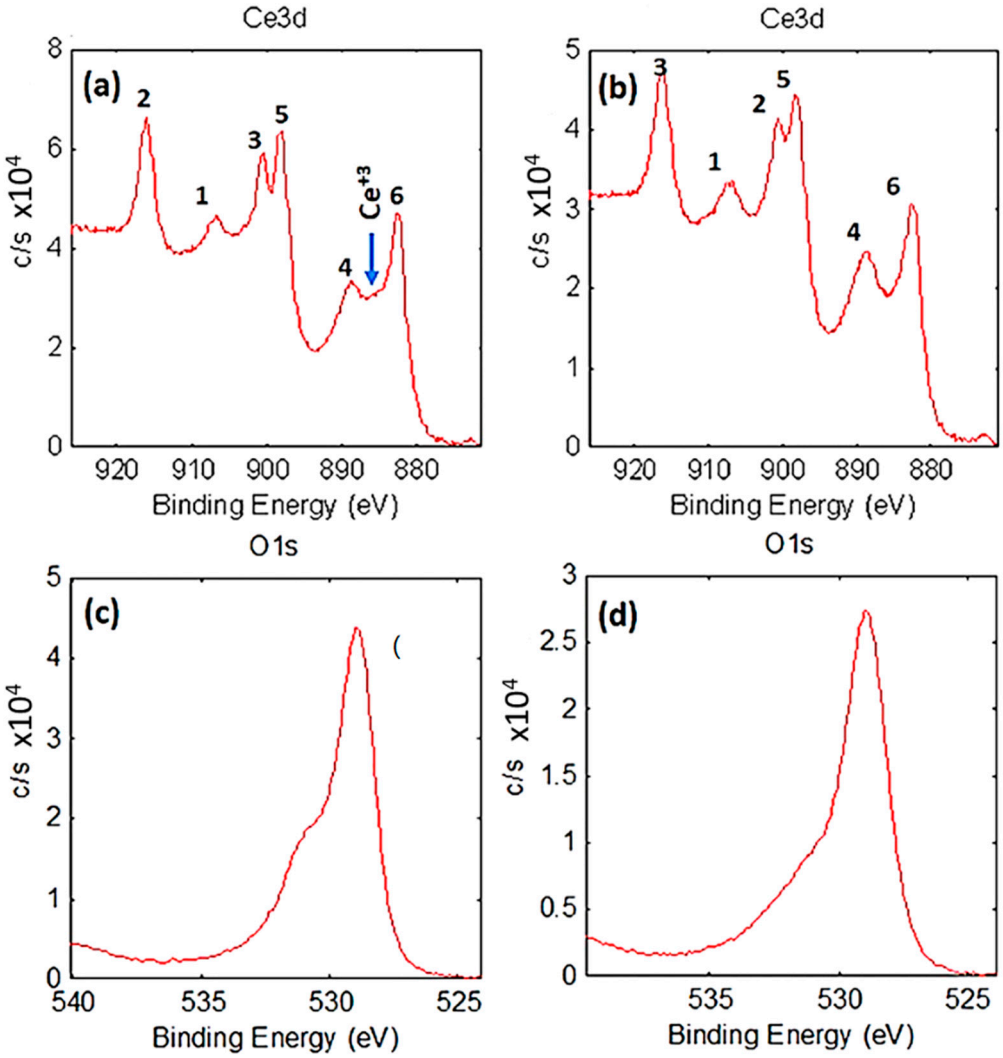

Figure 4. High-resolution of Ce 3d (including respective shake-up and shakedown peaks) and O 1s spectrum of fresh Au/CeO_2 prepared by LVCC (**a**,**c**) and DP (**b**,**d**), respectively.

Figure 5 shows a curve fitting of the Au 4f spectrum of the Au/CeO_2 nanoparticle catalyst prepared by physical and chemical methods. Two doublets were used in the curve fit of the Au 4f peak. One doublet at binding energies ~83.9 and ~87.6 eV was used to fit the Au. The second doublet at

~85.2 and ~88.9 eV was used to curve fit, possibly a trace of Au^{1+}. The DP sample had a broader Au 4f peak than the LVCC sample, as shown in Table 1.

Table 1. Comparison of the total Atom% of Au (Au^0 and Au^{1+}) at the surface of Au/CeO_2 catalysts prepared by LVCC and DP methods.

SAMPLE	Atom% Au	Atom% Au^0	Atom% Au^{1+}
Au/CeO_2 (LVCC)	0.3	0.282	0.018
Au/CeO_2 (DP)	1.2	0.8	0.4

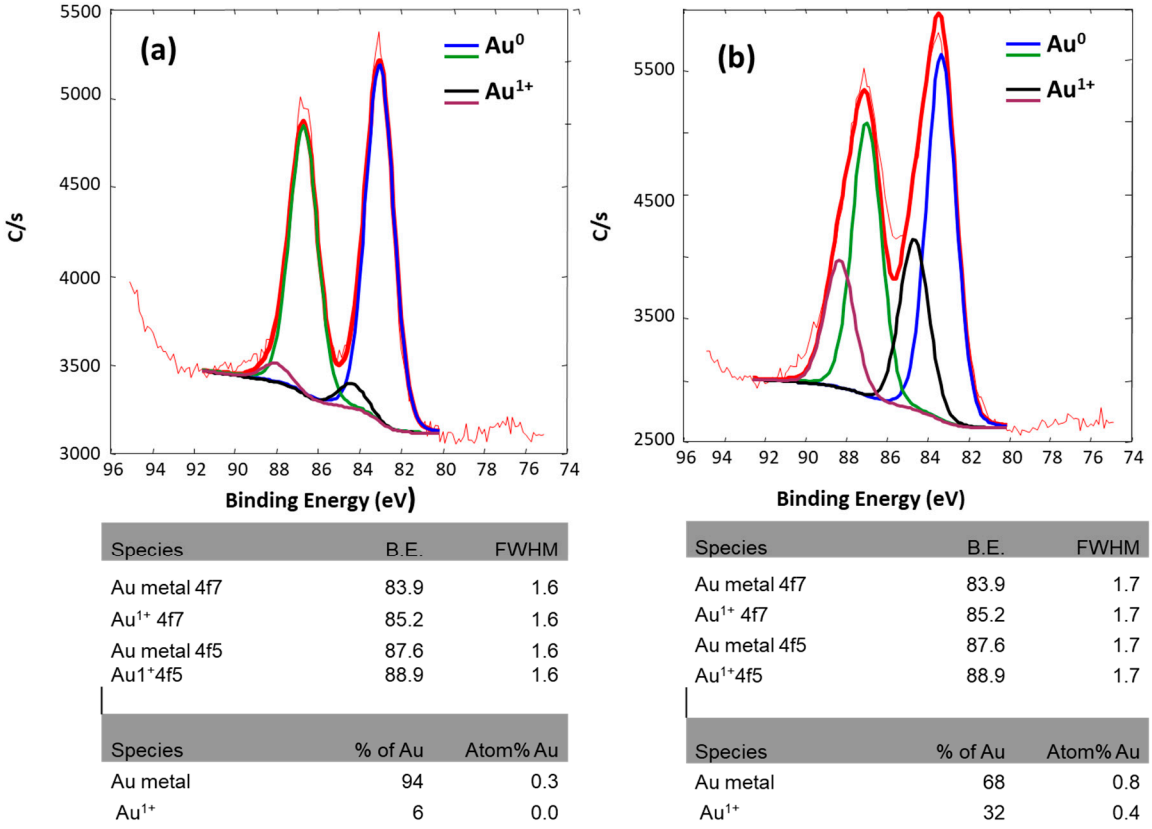

Species	B.E.	FWHM
Au metal 4f7	83.9	1.6
Au^{1+} 4f7	85.2	1.6
Au metal 4f5	87.6	1.6
$Au1^{+}$4f5	88.9	1.6

Species	% of Au	Atom% Au
Au metal	94	0.3
Au^{1+}	6	0.0

Species	B.E.	FWHM
Au metal 4f7	83.9	1.7
Au^{1+} 4f7	85.2	1.7
Au metal 4f5	87.6	1.7
Au^{1+}4f5	88.9	1.7

Species	% of Au	Atom% Au
Au metal	68	0.8
Au^{1+}	32	0.4

Figure 5. Curve fitting of Au 4f spectrum and relevant species of fresh 5% Au/CeO_2 prepared by (**a**) LVCC method and (**b**) DP method.

The curve fitting of both samples' Au 4f spectrum indicated that both contained mostly Au^0 and small amounts of Au^{1+} species. The XPS results revealed that the DP sample had a higher Au level and included more Au^{1+} than LVCC.

Based on the XPS and TEM results, it can be concluded that the Au in both samples was amorphous, most of Au was in the metallic state Au^0, and it formed a reliable solution of Au and CeO_2. However, the Au obtained by the chemical method was more amorphous, and some Au existed in the form of Au (OH), with an oxidation state of +1 [23].

2.1.5. Temperature Programmed Reduction (H_2-TPR) of Fresh Au/CeO_2

The Au's oxidation state was directly related to the interaction between Au and CeO_2, as indicated in the XPS results. To investigate the metal-support interaction between Au and CeO_2 support, we performed an H_2-TPR analysis. Furthermore, redox behaviors of the bare CeO_2 and Au/CeO_2 prepared via both methods were studied under H_2-TPR to investigate the interaction strength between

Au and CeO_2 in both samples. Figure 6 shows the H_2-TPR patterns of CeO_2 and Au/CeO_2 prepared by LVCC and DP methods. The TPR profile of CeO_2 exhibits two reduction peaks where the low-temperature reduction peak at 190 °C is attributed to the reduction of the surface oxygen of CeO_2 and the high-temperature peak at 487 °C is assigned to the decrease in the bulk oxygen of CeO_2.

However, the incorporation of Au significantly changed the TPR profiles. The results indicate that the high-temperature CeO_2 peak in the LVCC sample shifted to a lower temperature region with T_{max} around 451 °C; however, the high-temperature CeO_2 peak was not observable in the DP sample. A new feature appeared at the 219–385 °C temperature region—believed to have come from the reduction of the Ce-Au-O species. The presence of Ce-Au-O is supported by the XPS data, which shows the presence of traces of Ce^{3+} and Au^{1+}. The reduction of the Ce-Au-O enhanced the redox activity of Au-CeO_2. Similar results were reported for metallic Au, and other noble metals on CeO_2 promote the reduction of CeO_2 at extremely low temperatures due to spillover on the support [52]. It was reported that nanoparticles with high Au dispersion could increase the reducibility of the CeO_2 [27]. Other studies suggested that the surface oxygen's reducibility can be enhanced upon filling surface oxygen on CeO_2 lattices, such as Ce^{4+} sites with Au^{1+} or Au^{3+} ions and oxygen vacancies, thereby leading to more oxygen mobility and hence increased reducibility [53].

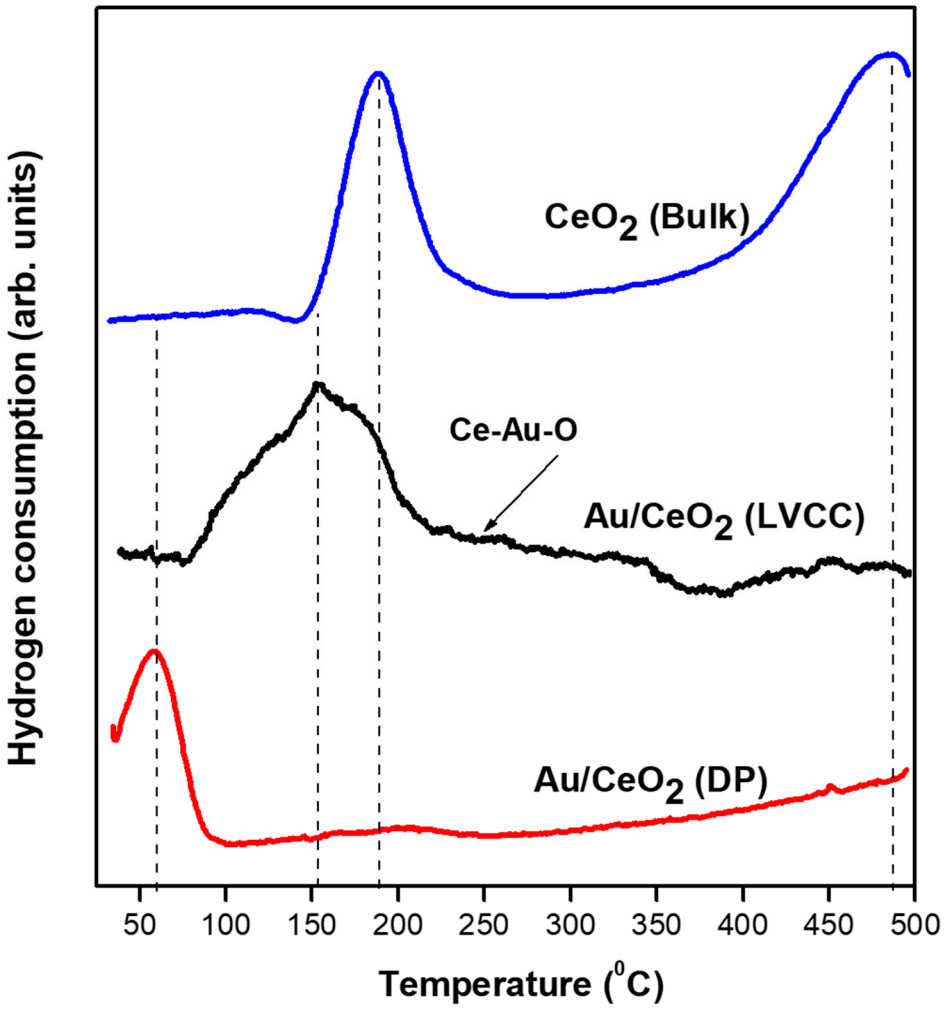

Figure 6. Temperature Programmed Reduction (TPR) patterns of CeO_2 bulk powder and as-synthesized Au/CeO_2 prepared by physical method (LVCC) and chemical method (DP).

2.2. Catalytic CO Oxidation Measurement

The Au/CeO_2 catalysts' activity as synthesized by physical and chemical methods was measured as a function of the catalyst temperature (first light-off). Table 2 summarizes the activities of both samples.

Table 2. Comparison of the catalytic activities of as-synthesized Au/CeO_2 (first light-off) prepared by LVCC and DP methods.

Sample 5% Au/CeO_2	3% Conversion (Light-Off) Temp. (°C)	50% Conversion Temp. (°C)	Maximum Conversion (%)	
			Temp. (°C)	Conversion
Physical (LVCC)	50.2	118.2	233.2	99.5
Chemical (DP)	0.1	14.7	110.0	100.0

Figure 7 represents a comparison between Au/CeO_2 activities developed by the two methods. Au/CeO_2 (DP)'s light-off temperature was 0.1 °C, and full conversion was reached at approximately 110 °C compared to the LVCC sample, which had a 50 °C temperature and reached complete conversion at 233 °C.

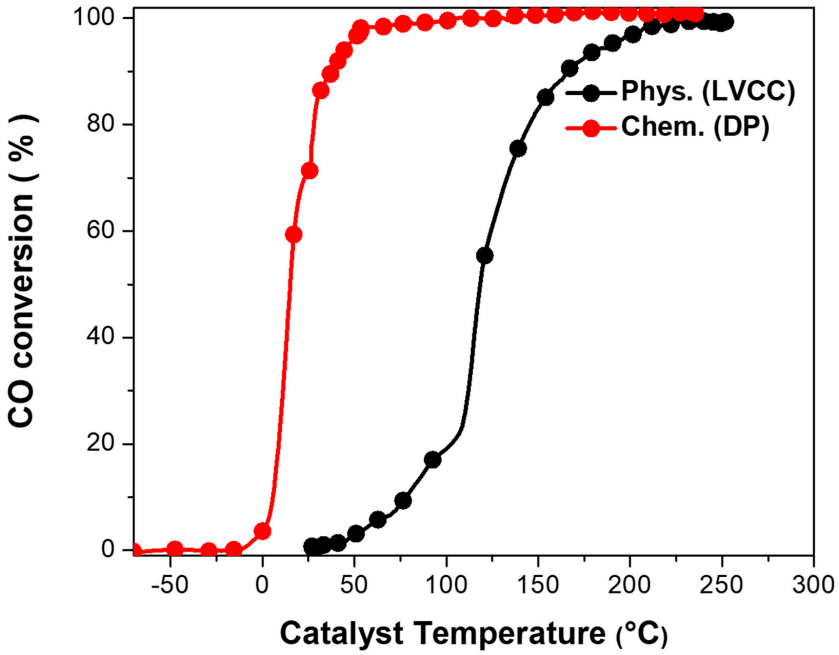

Figure 7. Comparison between activities of fresh Au/CeO_2 (first light-off) by a physical method (LVCC) and chemical method (DP). Sample mass = 10 mg, flow rate = 100 cc/min.

Based on both samples' catalytic activity and presence of higher Ce^{3+} and Au^{1+} in the XPS results combined and TPR profiles of Au/CeO_2, the appearance of significant oxygen vacancies on the surface of CeO_2 can be confirmed. These results lead to higher adsorption and reactive oxygen activation, which occurs at the Au nanoparticles and Au particles' step edges [49]. All these factors could explain the enhanced catalytic activity toward low-temperature CO oxidation. The results showed a direct correlation between the reduction temperature and the activity of the catalysts. The catalytic activity significantly increased as the reducibility of the Au-O-Ce of the surface in both catalysts—as evidenced by the H_2 consumption peak H_2-TPR curve—decreased. The electron transfer from Au nanoparticles to the CeO_2 surface led to the weakening of the Ce–O bond, which resulted in the activation of surface oxygen and the stabilization of Au atoms on the CeO_2 surface defect sites, leading to the lowered activation energy for CO oxidation. These results suggest that there was weak Au-CeO_2 interaction in

the LVCC sample. However, all the ceria in the DP sample, including the bulk ceria, reduced at 50 °C and below. The two peaks that characterize the ceria almost disappeared, and a new peak formed at room temperature. The high-intensity peak at room temperature could be attributed to the reduction of Au^{1+} to Au^{0} by removing the OH group. This result indicates that this catalyst has a strong Au-CeO_2 interaction (Strong Metal-Support Interaction (SMSI)) compared to the LVCC catalyst. These results demonstrate that both catalysts' light-off temperatures align well with reduction peaks −50 °C for the LVCC catalyst and approximately 0 °C for the DP catalyst.

The catalysts need to be in the reduced state to be active; the conversion aligns perfectly with the reduction temperatures shown in Figure 6.

2.3. Characterization of Au/CeO_2 Nanoparticle Catalyst after Heat Treatment in CO/O_2 Mixture (Second Light-Off)

To understand the change in the catalysts' performance and the origin of low-temperature catalytic activity shifts after the heat treatment, both catalysts were characterized using X-ray diffraction and TEM after catalysis. Figure 8 shows the X-ray diffraction patterns of Au/CeO_2 prepared by both methods after the heat treatment in the CO/O_2 mixture (second light-off). As expected, the CeO_2 support became crystalline in both catalysts. A full reflection of the crystalline metallic Au (JCPDS card no: 04-0784) could be observed in both catalysts by the presence of Au (111), Au (200), and Au (220) planes. The FWHM of CeO_2 (111) was 0.716 in the LVCC and 0.697 for the DP sample. The FWHM of Au (111) was 0.657 for both samples. However, the LVCC sample's intensity was 248.07, and that of the DP sample was 297.47, suggesting a slightly higher Au percentage in the latter.

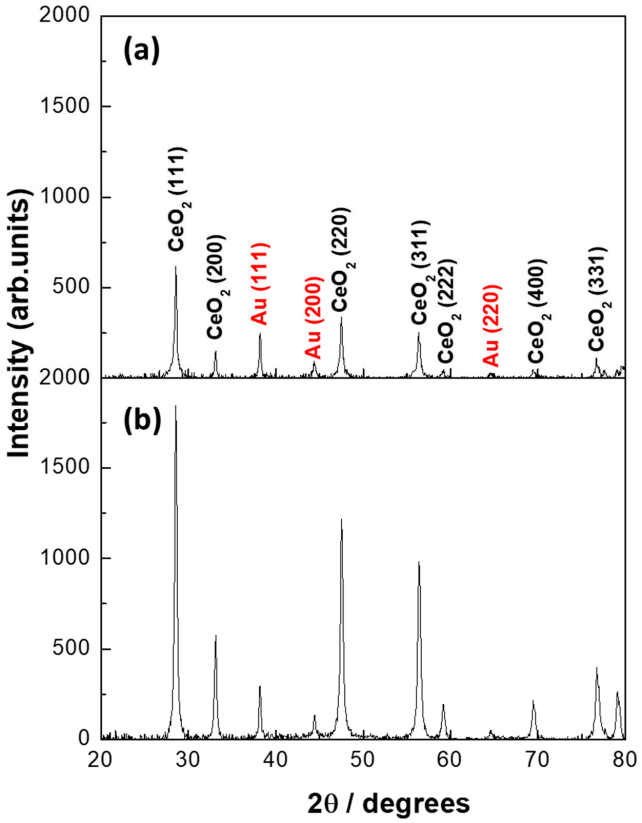

Figure 8. X-ray diffraction patterns of Au/CeO_2 catalysts prepared by (**a**) LVCC and (**b**) DP methods after heat treatment in the CO/O_2 mixture (second light-off).

To investigate the morphology of the catalysts after heat treatment, we performed TEM analysis, as shown in Figure 9, which revealed that both catalysts had developed utterly different

microstructures—a dispersion of metallic Au nanoparticles. Moreover, both samples showed the sintering of small Au particles into larger particles. Figure 9 shows the morphology and the particle size distribution of the Au/CeO_2 catalysts after heat treatment. Figure 9a–c shows TEM micrographs of the LVCC sample, indicating that the morphology of the LVCC sample was similar to that of the fresh sample, which consisted of small metallic Au, elongated CeO_2 particles (2–10 nm), and Au particles (5–25 nm) dispersed over large CeO_2 particles (50–500 nm). The Au particles had a size distribution of 1–25 nm and an average diameter of 11.6 nm. However, for the DP Figure 9d,e, two morphologies could be observed, consisting of small Au particles with narrow size distribution (2–6 nm) with an average diameter of 5 nm dispersed over large CeO_2 particles, and two-dimensional Au clusters on CeO_2 particles, which could be observed through the X-ray diffraction patterns. These particles were supported on highly crystalline CeO_2 particles with sizes ranging from 50 nm to 500 nm. The results also suggest that minor sintering of Au and CeO_2 nanoparticles took place in both catalysts. However, the LVCC sample showed more sintering than the DP sample, which explains the increase in the intensity of Au peaks in both catalysts and the detection of Au in the DP sample. Similar results were reported by Wagner et al. [54].

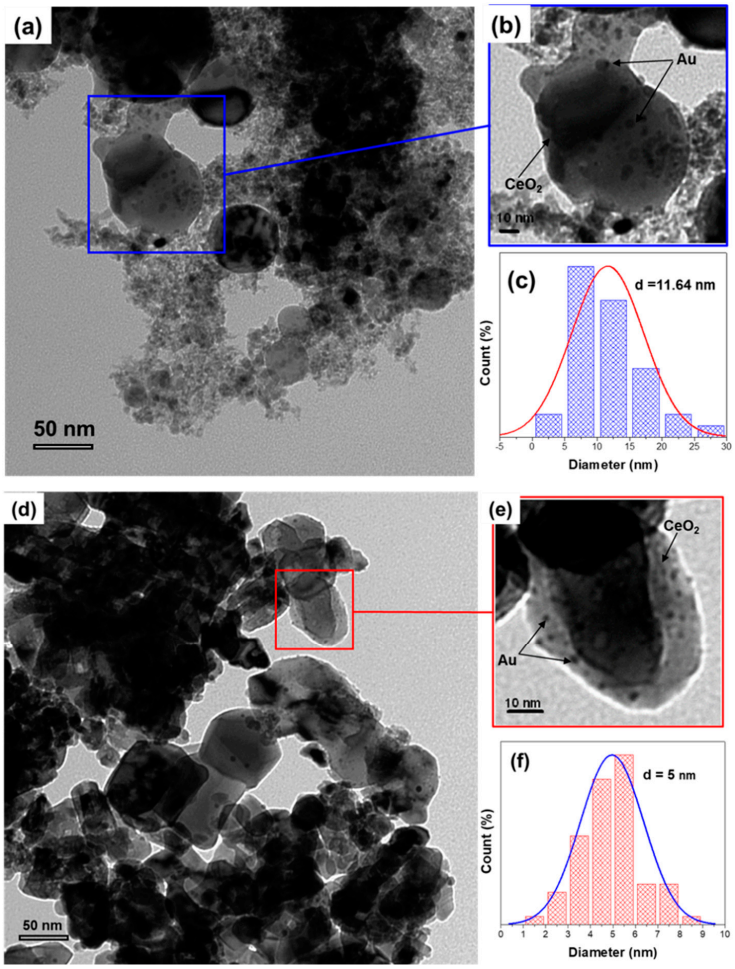

Figure 9. TEM micrographs and particle size distribution of Au/CeO_2 prepared by the physical method (LVCC) (**a**–**c**) and the chemical method (DP) (**d**–**f**)., after the heat treatment in the CO/O_2 mixture (second light-off), the light-off temperature was shifted for both catalysts—from 50 °C to 27 °C for the LVCC catalyst and from 0.1 °C to 28 °C for the DP catalyst—as shown in Figure 8. Table 3 shows the activities of Au/CeO_2 prepared by physical and chemical methods after heat treatment in the CO/O_2 mixture (second light-off).

Table 3. Catalytic activities of Au/CeO_2 prepared by LVCC and DP methods after heat treatment in the CO/O_2 mixture (second light-off).

Sample 5% Au/CeO_2	3% Conversion (Light-Off) Temp. (°C)	50% Conversion Temp. (°C)	Maximum Conversion (%)	
			Temp. (°C)	Conversion
Physical (LVCC)	27.5	89.95	210.9	99.4
Chemical (DP)	−28.3	19.2	178.3	100.0

Figure 10 shows the light-off temperatures of both catalysts after the heat treatment in CO/O_2. The results revealed that the conversion curve for both samples had significantly shifted toward the low temperature. This shift could be attributed to removing moisture and impurities (i.e., hydrocarbons) from the catalyst surface and Au precipitation in the $Au\text{-}CeO_2$ interface to the surface, which increased the metal-support interaction.

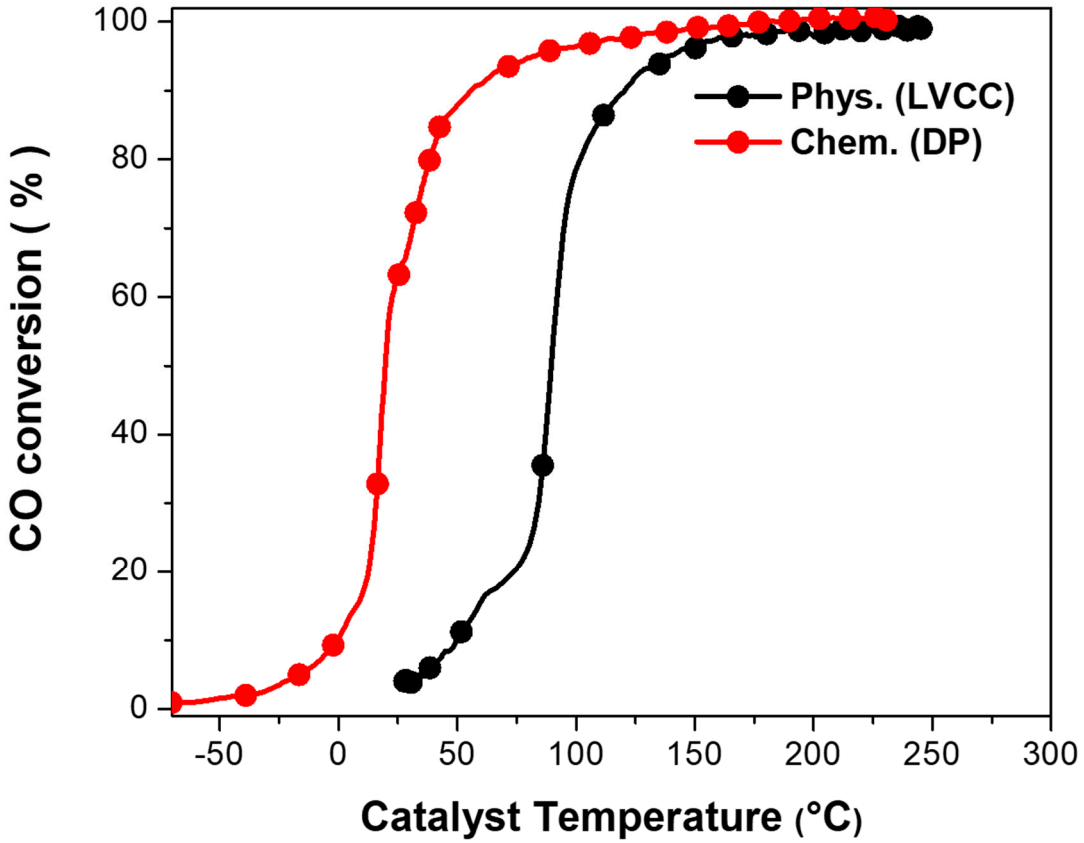

Figure 10. Comparison between Au/CeO_2 activities after heat treatment in CO/O_2 mixture prepared by LVCC and DP methods. Sample mass = 10 mg, flow rate = 100 cc/min.

3. Methods

3.1. Experimental Method

The CO oxidation catalytic activity of Au-metal oxide catalysts varies by varying the support and is highly dependent on the preparation method, reaction conditions, and the pre-treatment conditions. We employed chemical and physical methods to produce highly active Au/CeO_2 nanoparticle catalysts in this work. LVCC was used as an example of a physical method, and DP was used as an example of a chemical method.

3.2. Catalyst Preparation

3.2.1. Physical Method (Laser Vaporization Controlled Condensation (LVCC))

Different physical methods, such as sputtering, chemical vapor deposition, exploding wire, and One-Pot laser vaporization-controlled condensation [55], are used to produce nanoparticles from the vapor phase. These methods are based on the condensation of supersaturated metal vapors. In this context, LVCC has an advantage over typical thermal vaporization methods due to the production of a high-density vapor of any metal or metal oxide targets. The benefits of the vapor phase synthesis include the contamination-free products (as compared to chemical reductions in solutions), the elimination of chemical precursors and solvents, and, in most cases, the production of highly crystalline nanoparticles [56–58]. El-Shall et al. introduced the LVCC method and demonstrated its use in producing nanoparticles with unique surface oxidation, photochromic, and photoluminescence properties [59]. In the LVCC method, a target consisting of metal/metal oxide powders is made into a pallet and placed on the lower plate of a diffusion cloud chamber (DCC); the chamber is filled with a pure carrier gas such as He or Ar or a mixture containing a known concentration of reactant gas such as O_2. A pulsed beam of the second harmonic (532 nm) Nd-YAG laser operated at 30 Hz (50–200 mJ/pulse laser power, 5 or 10 ns pulse duration) is focused on a target of interest. The target is placed in a chamber with well-defined temperature and pressure. The chamber consists of two flat, circular stainless-steel plates separated by a class ring. The target is placed on the bottom plate, where the temperature is maintained higher than the top plate and controlled by circulating water. The top plate can be cooled to 150 K using liquid N_2. The advantage of the temperature gradient between the two plates is creating a convection current; this current is further enhanced by using a dense carrier gas under high pressure (10^3 torrs). The pulsed metal vapor is generated by laser vaporization of the target. The laser beam is moved on the target surface to expose new surface areas to achieve good reproducibility of the amount of vapor produced. After the laser pulse strikes the target and creates plasma, the ejected pulse of metal atoms interacts with the gas inside the chamber. Nucleation takes place immediately and results in the formation of nanoparticles. Finally, diffusion and convection currents prevent the particles from growing larger by removing them from the high-density nucleation zone.

In a typical synthesis, a commercial micron-sized Au commercial powder (mean particle size < 2-micron, purity 99.95%, Sigma-Aldrich, St. Louis, MO, USA) and Cerium (IV) oxide commercial powder (<5 µm, 99.9%, Sigma-Aldrich, St. Louis, MO, USA) were used to prepare compressed pellet targets of selected compositions of the catalyst/support (Au/CeO_2), with known compositions. Samples were prepared with different wt% (2%, 5%, and 10%) of Au in Au/CeO_2. The Au/CeO_2 powder target was placed on the lower plate of a diffusion cloud chamber (DCC) with He (99.99%) carrier gas; this was followed by vaporizing the target using second harmonic generation (532 nm) Nd-YAG laser (30–50 mJ/pulse, 10 ns pulse duration). The steady convective current resulting from the temperature gradient between the lower and top plates of the DCC removed the Au/CeO_2 nanoparticles from the vaporization zone rapidly before they could grow into larger particles. The resulting $AuCeO_2$ nanoparticles deposited on the cold top plate consisting of small Au nanoparticles homogeneously dispersed on larger nanoparticle oxide support surfaces were collected.

We found that 5% of Au metal loading yields the highest catalytic activity, as shown in Figure S1. Therefore, we used the Au/CeO_2 sample with 5% Au. The Au loading in this study was synthesized by mixing 5% Au powder with 95% CeO_2 powder.

Although many catalysts prepared by the LVCC method show higher catalytic activity than other conventional catalysts, the LVCC method has certain disadvantages, such as low yield compared to chemical methods. As an alternative method to produce a large amount of the catalyst, 5% Au/CeO_2 was prepared using chemical methods—in this case, the Deposition-Precipitation (DP) method.

3.2.2. Chemical Method (Deposition-Precipitation (DP))

To synthesize the Au/CeO_2 sample with 5% Au using the DP method, the Au precursor was introduced onto the CeO_2 support using the DP method [60]. In a typical synthesis, 0.885 g (equivalent to 5% Au) of Hydrogen Tetrachloroaurate (III) Hydrate ($HAuCl_4$, 99.99% Sigma Aldrich, St. Louis, MO, USA) was dissolved in water and slowly and homogeneously precipitated by the hydroxide ion from NaOH solution with a pH between 6 and 10. Cerium (IV) oxide commercial powder (<5 µm, 99.9%, Sigma-Aldrich, St. Louis, MO, USA) (4.75 g) (equivalent to 95% Au) was suspended in water with pH between 6 and 10 by adding the NaOH solution dropwise and stirring for one hour; then, the $HAuCl_4$ solution was added to the CeO_2 solution dropwise; controlling the pH between 6 and 10 by adding NaOH. As a result, the Au $(OH)_3$ precursor was deposited exclusively on the surface of CeO_2. Then the solution was filtered to obtain Au $(OH)_3/CeO_2$ particles followed by washing, drying, and then heating at 105 °C for one hour to produce Au metal on CeO_2 nanoparticles.

3.3. Catalyst Characterization

The catalysts' surface area was measured using the five-point N_2 physisorption process detailed in the Brunauer–Emmett–Teller technique (BET) (Quantachrome Autosorb Automated Gas Sorption Unit). Elemental analysis of the samples was performed using Inductively Coupled Plasma Optical Emission Spectroscopy (ICP-OES Thermo Scientific iCAP 6500 ICP Spectrometer, (Waltham, MA, USA).

The catalyst's crystallographic structure was analyzed using X-ray diffraction (XRD) (Philips X'Pert Pro Theta-Theta system (Westborough, MA, USA) operated at 45 kV and tube current of 40 mA). Scanning Electron Microscopy (SEM) was done using a Quantum DS-130S electron microscope. The transmission electron microscope (TEM) images were obtained using a JOEL JEM-FXII TEM operated at 200 kV. High-resolution TEM images were obtained using a JOEL 4000EX (JEOL, Tokyo, Japan) operated at 400 kV. A drop of methanol-dispersed nanoparticles was placed on a carbon-coated copper grid and left to dry. X-ray Photon-Electron Spectroscopy (XPS) spectra were obtained using the Physical Electronics Model 5700LSci ESCA spectrometer (Chanhassen, MN, USA) (with monochromatic aluminum), operated at 350 watts, with Charge correction C-(C, H) in C 1s spectra at 284.8 eV. Temperature Programmed Reduction (TPR) profiles were obtained using the EPA Cincinnati AutoChem II 2920 V2 (Norcross, GA, USA).

3.4. Catalytic Activity Measurements

The catalyst's catalytic activity measurements were performed at atmospheric pressure in a quartz tube flow reactor (length 50 cm, i.d. 0.9 cm) coupled with an infrared detector described elsewhere [38]. In a typical measurement, 10 mg of the catalyst is placed in a fixed bed between two quartz wool pieces placed in the middle of a quartz tube. The flow tube is then placed inside a temperature programmer Thermolyne 2100 tube furnace. The sample temperature is monitored using an Omega K-type thermocouple inserted in the middle of the sample. Another thermocouple is built into the furnace to measure the furnace temperature. A LabVIEW-based program recorded the temperatures and the concentration data. The sample temperature is always higher than the furnace temperature since the catalytic oxidation reaction of CO is exothermic. Therefore, all the data in this work are plotted as a function of the sample or reaction temperatures.

The gas mixture flow rate was controlled by **MKS Instruments** digital mass flow meters. The effluent gases were analyzed using an Automated Custom System infrared gas analyzer. In these experiments, a gas mixture containing 3.60 vol% of CO and 20.0 vol% of O_2 balanced with helium was used. The mixture flowed over the catalyst (100 cc/min) while the catalyst was heated to different temperatures. The effluent gases were introduced to the infrared gas analyzer. CO and CO_2 concentrations were measured based on the absorption of IR radiation. By monitoring the change of the CO and CO_2 concentrations and plotting the normalized ratio $([CO]/[CO] + [CO_2]) \times 100\%)]$ as a function of catalyst temperature, the catalyst activity can be measured.

4. Long-Term Catalyst Stability of Au/CeO_2 Catalysts Prepared by LVCC and DP Methods

To investigate the long-term catalytic stability and regeneration of both catalysts' active sites, we heated the catalysts to the temperature that corresponded to 50% and 100% CO conversion and kept the catalysts at that temperature while allowing the gas mixture to flow continuously over the catalyst bed. The catalytic activity of Au/CeO_2 catalysts prepared by LVCC and DP methods were measured as a function of time on the stream by keeping the temperature constant at 118.5 °C for the LVCC sample and 15 °C for the DP sample, which corresponded to 50% CO conversion and at 234 °C for the LVCC sample and 110 °C for the DP sample, which corresponded to 100% CO conversion, while the CO/O_2 mixture flowed over Au/CeO_2, as shown in Figure 11. Both catalysts showed excellent stability for more than 14 h. However, the LVCC catalyst showed slightly better stability than the DP catalyst. This stability was demonstrated by the regeneration of the active sites and constant conversion percentage of 50% or 100% even after 14 h of continuous use. Long-term stability tests showed that the catalysts showed higher stability at 50% due to fluctuation of catalytic activity than at 100% due to catalyst surface variations, such as sintering, at high temperatures.

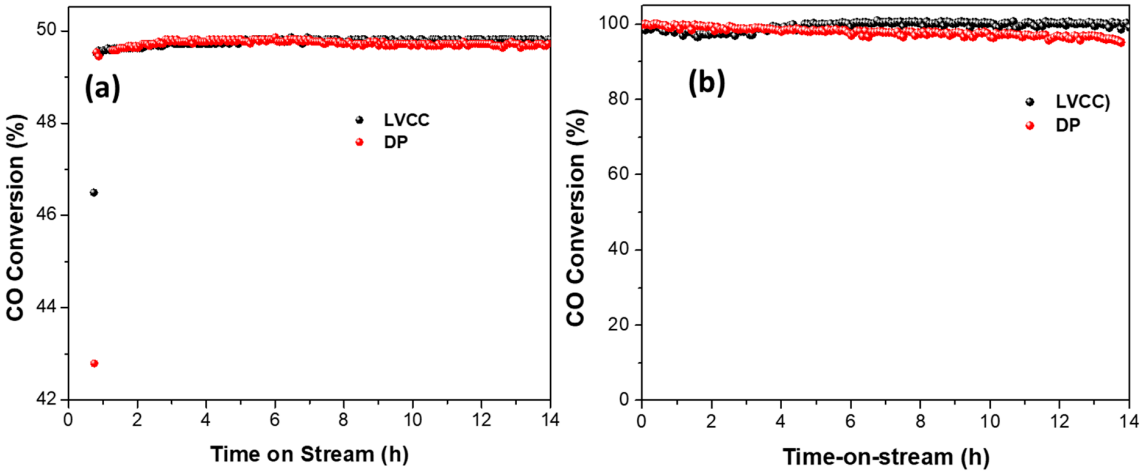

Figure 11. Long-term stability of Au/CeO_2 prepared by LVCC and DP methods at (**a**) 50% conversion and (**b**) 100% conversion. Sample mass = 10 mg, flow rate = 100 cc/min.

Our results showed that the LVCC catalyst had a large surface area compared to the DP catalyst; the LVCC catalyst showed lower CO conversion activity than the DP catalyst. These results could be attributed to the larger particle size, weaker metal-support interaction, and low Au dispersion. On the other hand, the DP catalyst showed higher CO conversion where small-sized nanoparticles were required, and high dispersion was necessary to create a robust metal-support interaction, leading to increased reducibility. These results are confirmed by XRD and TEM techniques, where the LVCC sample's surface area was higher due to the small Au particle size (<10 nm) and high dispersion and the fact that that many of these particles cannot be detected as the spectrometer's detection limits are less than 3 nm.

The DP method showed activity below room temperature similar to that in the Au/TiO_2 catalysts reported by Haruta and in the Au/Fe_2O_3 catalysts [55]. The modification of support can help stabilize and enhance the activity toward other reactions such as methanol oxidation [61]. Reaction mechanisms of CO oxidation on Au/TiO_2 catalysts have been reported by Haruta et al. [62]. They suggest that the reaction takes place on Au surfaces at the steps, edges, and corners of Au particles with an activation energy of 0 kJ/mol (below 300 K). At temperatures above 300 K, the reaction takes place at the perimeter interfaces, where CO is adsorbed on the surfaces of Au nanoparticles, and the molecular oxygen is adsorbed at the support interface with an activation energy of 0 kJ/mol, and it proceeds faster. These results are in good agreement with results obtained for Au supported on reducible oxides such

as TiO_2 support, where the catalytic activities below room temperature are mainly attributed to the fact that the reaction takes place on Au surfaces at the steps, edges, and corners with 0 kJ/mol activation energy [15,17,61–63].

Furthermore, recent experimental evidence suggests that the presence of Au^{1+} plays a crucial role in the activity of Au/CeO_2. The presence of isolated Au adatoms or Au cations in $Au_xCe_{1-x}O_2$ facilitates the CO oxidation with no activation energy through the formation of surface oxygen vacancies followed by the adsorption of molecular oxygen vacancies—thereby forming oxygen species, which catalyze the molecular CO oxidation, leading to the recovery of the stoichiometric $Au_xCe_{1-x}O_2$. The CeO_2 surface is shown to induce charge transfer at the Au-CeO_2 interface, which leads to the reduction of CeO_2 support and in lattice Ce^{3+} and surface Au^{1+} ions where the molecular spillover enhances the CO oxidation reaction from the Au^{1+} adatom to the CeO_2 surface support [64].

In addition to the XPS and TPR results, and based on the results obtained by Haruta et al., the difference in the LVCC and DP samples' catalytic activity can be explained based on how the Au nanoparticles are set on the support and the length of the interface between them. Tana et al. concluded that the Au/CeO_2 interface, which is determined by the Au particles' size, plays a vital role in achieving high reactivity [65]. The results are consistent with the results reported by Zhou et al., where they attributed the enhanced activity toward CO oxidation reaction and found that the rate is scaled with the total length of the Au/CeO_2 interfaces [65–67]. In the physical method, however, the interface is shorter than that in the chemical method, which indicates that the interaction is stronger in the chemical method, and hence the catalytic activity is higher.

5. Conclusions

This study demonstrates that the synthesis method (physical vs. chemical) can affect the size, morphology, dispersion, reducibility, nature surface active site, and the Au/CeO_2 nanoparticle catalyst's catalytic properties. The characterization data and catalytic CO oxidation results reported in this paper reveal the successful synthesis of crystalline Au nanoparticles—with a size of 3–10 nm for the LVCC method and 3–5 nm for the DP method supported—on crystalline CeO_2. Additionally, it showed that the stability and dispersion of Au nanoparticles on the CeO_2 surface, coupled with the redox properties of CeO_2, results in Strong Metal-Support Interaction (SMSI) at the interface between Au and CeO_2, thereby leading to the formation of unique active surface sites capable of activating both CO and O_2 simultaneously.

The two catalysts fully converted CO to CO_2 at a temperature of less than 120 °C. The catalyst's high catalytic performance, which was ascribed to structural properties, supports oxygen storage capacity and Au particles' dispersion on the support. The type of active sites (Au^{1+} or Au^0) was found to influence the catalytic activity. However, the DP sample had a high activity for CO oxidation, even at temperatures below −10 °C, while the LVCC sample, which contained only metallic gold, light-off at room temperature. The enhanced catalytic activity of the Au/CeO_2 catalyst is attributed to the strong interaction of Au with CeO_2, where Au can promote the reduction of Ce^{4+} to Ce^{3+} and thus facilitate the charge transfer from Au to CeO_2, which results in a higher oxidation state of Au and hence increases the oxygen storage capacity of CeO_2. Compared with the physical method (LVCC), the chemical method (DP) showed superior activities, which can be attributed to creating small and well-dispersed Au nanoparticles and forming a unique interface that enhances the synergetic effects between Au and CeO_2. This effect results from the electron transfer and strong interaction between the Au surface species (Au^{1+}) and the stable and reducible underlying CeO_2 support. These results suggest that the catalytic activity is highly dependent on the nature of the active site, which is determined by a combination of the particle size, morphology, and the interface between Au nanoparticles and the CeO_2 support. The catalytic activity below room temperature of the DP catalyst can mainly be attributed to the fact that the CO oxidation occurs on the interface and defect sites (adatoms, steps, edges, and corners) of the Au surface where the CO oxidation reaction proceeds with 0 kJ/mol activation energy.

Supplementary Materials: The following are available online at http://www.mdpi.com/2073-4344/10/11/1351/s1.

Author Contributions: K.M.S. wrote and edited the entire paper and oversaw the quality of the selected literature and the flow of the paper, and M.S.E.-S. managed and participated in the quality of the manuscript. The authors worked together to prepare this manuscript. All authors have read and agreed to the published version of the manuscript.

Funding: This research received no external funding.

Conflicts of Interest: The authors declare no conflict of interest.

References

1. McCrea, K.R.; Parker, J.S.; Somorjai, G.A. The Role of Carbon Deposition from CO Dissociation on Platinum Crystal Surfaces during Catalytic CO Oxidation: Effects on Turnover Rate, Ignition Temperature, and Vibrational Spectra. *J. Phys. Chem. B* **2002**, *106*, 10854–10863. [CrossRef]
2. Valden, M.; Lai, X.; Goodman, D.W. Onset of catalytic activity of gold clusters on titania with the appearance of nonmetallic properties. *Science* **1998**, *281*, 1647–1650. [CrossRef] [PubMed]
3. Haruta, M.; Yamada, N.; Kobayashi, T.; Iijima, S. Gold catalysts prepared by coprecipitation for low-temperature oxidation of hydrogen and of carbon monoxide. *J. Catal.* **1989**, *115*, 301–309. [CrossRef]
4. Al Soubaihi, R.M.; Saoud, K.M.; Ye, F.; Zar Myint, M.T.; Saeed, S.; Dutta, J. Synthesis of hierarchically porous silica aerogel supported Palladium catalyst for low-temperature CO oxidation under ignition/extinction conditions. *Microporous Mesoporous Mater.* **2020**, *292*, 109758. [CrossRef]
5. Bond, G.C.; Thompson, D.T. *Catalysis by Gold*; Catalysis Reviews; World Scientific: Singapore, 1999; Volume 41, pp. 319–388.
6. Su, F.Z.; Liu, Y.M.; Wang, L.C.; Cao, Y.; He, H.Y.; Fan, K.N. Ga–Al Mixed-Oxide-Supported Gold Nanoparticles with Enhanced Activity for Aerobic Alcohol Oxidation. *Angew. Chem. Int. Ed.* **2008**, *47*, 334–337. [CrossRef]
7. Haruta, M.; Tsubota, S.; Kobayashi, T.; Kageyama, H.; Genet, M.J.; Delmon, B. Low-Temperature Oxidation of CO over Gold Supported on TiO_2, α-Fe_2O_3, and Co_3O_4. *J. Catal.* **1993**, *144*, 175–192. [CrossRef]
8. Abdelsayed, V.; Saoud, K.M.; El-Shall, M.S. Vapor phase synthesis and characterization of bimetallic alloy and supported nanoparticle catalysts. *J. Nanoparticle Res.* **2006**, *8*, 519–531. [CrossRef]
9. Min, B.K.; Friend, C.M. Heterogeneous Gold-Based Catalysis for Green Chemistry: Low-Temperature CO Oxidation and Propene Oxidation. *Chem. Rev.* **2007**, *107*, 2709–2724. [CrossRef]
10. Alhumaimess, M.; Aldosari, O.; Alshammari, H.; Kamel, M.M.; Betiha, M.A.; Hassan, H.M. Ionic liquid green synthesis of CeO_2 nanorods and nano-cubes: Investigation of the shape dependent on catalytic performance. *J. Mol. Liq.* **2019**, *279*, 649–656. [CrossRef]
11. Chen, T.; Xie, Z.; Jiang, W.; Jiang, W.; Zhang, X.; Liu, J. Synthesis of CeO_2 nanosheets with a room temperature ionic liquid assisted method. *J. Adv. Ceram.* **2016**, *5*, 111–116. [CrossRef]
12. Sun, Y.; Liu, W.; Tian, M.; Wang, L.; Wang, Z. A Rational Design of the Sintering-Resistant Au-CeO_2 Nanoparticles Catalysts for CO Oxidation: The Influence of H_2 Pretreatments. *Materials* **2018**, *11*, 1952. [CrossRef] [PubMed]
13. Kim, H.J.; Jang, M.G.; Shin, D.; Han, J.W. Design of Ceria Catalysts for Low-Temperature CO Oxidation. *ChemCatChem* **2020**, *12*, 11–26. [CrossRef]
14. Reveles, J.U.; Saoud, K.M.; El-Shall, M.S. Water inhibits CO oxidation on gold cations in the gas phase. Structures and binding energies of the sequential addition of CO, H_2O, O_2, and N_2 onto Au^+. *Phys. Chem. Chem. Phys.* **2016**, *18*, 28606–28616. [CrossRef] [PubMed]
15. Ishida, T.; Murayama, T.; Taketoshi, A.; Haruta, M. Importance of Size and Contact Structure of Gold Nanoparticles for the Genesis of Unique Catalytic Processes. *Chem. Rev.* **2019**, *120*, 464–525. [CrossRef]
16. Saavedra, J.; Doan, H.A.; Pursell, C.J.; Grabow, L.C.; Chandler, B.D. The critical role of water at the gold-titania interface in catalytic CO oxidation. *Science* **2014**, *345*, 1599–1602. [CrossRef] [PubMed]
17. Tada, K.; Maeda, Y.; Koga, H.; Okumura, M. TiO_2 Crystal Structure Dependence of Low-temperature CO Oxidation Catalyzed by Au/TiO_2. *Chem. Lett.* **2018**, *47*, 200–203. [CrossRef]
18. Duan, Z.; Henkelman, G. Calculations of CO Oxidation over a Au/TiO_2 Catalyst: A Study of Active Sites, Catalyst Deactivation, and Moisture Effects. *ACS Catal.* **2018**, *8*, 1376–1383. [CrossRef]
19. Bunluesin, T.; Cordatos, H.; Gorte, R.J. Study of CO Oxidation Kinetics on Rh/Ceria. *J. Catal.* **1995**, *157*, 222–226. [CrossRef]

20. Bunluesin, T.; Putna, E.S.; Gorte, R.J. A comparison of CO oxidation on ceria-supported Pt, Pd, and Rh. *Catal. Lett.* **1996**, *41*, 1–5. [CrossRef]
21. Li, L.; Liu, Y.; Wang, Q.; Zhou, X.; Li, J.; Song, S.; Zhang, H. CeO_2 supported low-loading Au as an enhanced catalyst for low temperature oxidation of carbon monoxide. *CrystEngComm* **2019**, *21*, 7108–7113. [CrossRef]
22. Al Soubaihi, R.; Saoud, K.; Dutta, J. Critical Review of Low-Temperature CO Oxidation and Hysteresis Phenomenon on Heterogeneous Catalysts. *Catalysts* **2018**, *8*, 660. [CrossRef]
23. Huang, X.S.; Sun, H.; Wang, L.C.; Liu, Y.M.; Fan, K.N.; Cao, Y. Morphology effects of nanoscale ceria on the activity of Au/CeO_2 catalysts for low-temperature CO oxidation. *Appl. Catal. B Environ.* **2009**, *90*, 224–232. [CrossRef]
24. Si, R.; Flytzani-Stephanopoulos, M. Shape and Crystal-Plane Effects of Nanoscale Ceria on the Activity of Au-CeO_2 Catalysts for the Water–Gas Shift Reaction. *Angew. Chem.* **2008**, *120*, 2926–2929. [CrossRef]
25. Carrettin, S.; Concepción, P.; Corma, A.; Lopez Nieto, J.M.; Puntes, V.F. Nanocrystalline CeO_2 Increases the Activity of Au for CO Oxidation by Two Orders of Magnitude. *Angew. Chem. Int. Ed.* **2004**, *43*, 2538–2540. [CrossRef]
26. Zhang, X.; Duan, D.; Li, G.; Feng, W.; Yang, S.; Sun, Z. Monolithic Au/CeO_2 nanorod framework catalyst prepared by dealloying for low-temperature CO oxidation. *Nanotechnology* **2018**, *29*, 095606. [CrossRef]
27. Luo, J.; Liu, Y.; Niu, Y.; Jiang, Q.; Huang, R.; Zhang, B.; Su, D. Insight into the chemical adsorption properties of CO molecules supported on Au or Cu and hybridized Au-CuO nanoparticles. *Nanoscale* **2017**, *9*, 15033–15043. [CrossRef]
28. Palomino, R.M.; Gutiérrez, R.A.; Liu, Z.; Tenney, S.; Grinter, D.C.; Crumlin, E.; Waluyo, I.; Ramírez, P.J.; Rodriguez, J.A.; Senanayake, S.D. Inverse Catalysts for CO Oxidation: Enhanced Oxide-Metal Interactions in MgO/Au(111), CeO_2/Au(111), and TiO_2/Au(111). *ACS Sustain. Chem. Eng.* **2017**, *5*, 10783–10791. [CrossRef]
29. Yinga, F.; Wang, S.; Au, C.-T.; Lai, S.-Y. Effect of the oxidation state of gold on the complete oxidation of isobutane on Au/CeO_2 catalysts. *Gold Bull.* **2010**, *43*, 241–251. [CrossRef]
30. Fu, Q.; Weber, A.; Flytzani-Stephanopoulos, M. Nanostructured Au–CeO_2 catalysts for low-temperature water–gas shift. *Catal. Lett.* **2001**, *77*, 1–3. [CrossRef]
31. He, Y.; Du, S.; Li, J.; Zhang, R.; Liang, X.; Chen, B. Mesoporous Ceria-Supported Gold Catalysts Self-Assembled from Monodispersed Ceria Nanoparticles and Nanocubes: A Study of the Crystal Plane Effect for the Low-Temperature Water Gas Shift Reaction. *Chemcatchem* **2017**, *9*, 4070–4082. [CrossRef]
32. Yu, H.; Jiao, Y.; Li, N.; Pang, J.; Li, W.; Zhang, X.; Li, X.; Li, C. Au-CeO_2 Janus-like nanoparticles fabricated by block copolymer templates and their catalytic activity in the degradation of methyl orange. *Appl. Surf. Sci.* **2018**, *427*, 771–778. [CrossRef]
33. Scire, S.; Minico, S.; Crisafulli, C.; Pistone, A. Catalytic combustion of volatile organic compounds on gold/cerium oxide catalysts. *Appl. Catal. B Gen.* **2003**, *40*, 43–49. [CrossRef]
34. Luengnaruemitchai, A.; Osuwan, S.; Gulari, E. Comparative studies of low-temperature water–gas shift reaction over Pt/CeO_2, Au/CeO_2, and Au/Fe_2O_3 catalysts. *Catal. Commun.* **2003**, *4*, 215–221. [CrossRef]
35. Delmon, B.; Grange, P.; Jacobs, P.A.; Poncelet, G. Foreword. In Preparation of Catalysts V-Scientific Bases for the Preparation of Heterogeneous Catalysts. In *Proceedings of the Fifth International Symposium*; Elsevier: Amsterdam, The Netherlands, 1991; pp. xi–xii.
36. Wolf, A.; Schuth, F. A systematic study of the synthesis conditions for the preparation of highly active gold catalysts. *Appl. Catal. A* **2002**, *226*, 1–13. [CrossRef]
37. Li, J.; Li, W. Effect of preparation method on the catalytic activity of Au/CeO_2 for VOCs oxidation. *J. Rare Earths* **2010**, *28*, 547–551. [CrossRef]
38. Glaspell, G.; Abdelsayed, V.; Saoud, K.M.; El-Shall, M.S. Vapor-phase synthesis of metallic and intermetallic nanoparticles and nanowires: Magnetic and catalytic properties. *Pure Appl. Chem.* **2006**, *78*, 1667–1689. [CrossRef]
39. Yang, Y.; Saoud, K.M.; Abdelsayed, V.; Glaspell, G.; Deevi, S.; El-Shall, M.S. Vapor phase synthesis of supported Pd, Au, and unsupported bimetallic nanoparticle catalysts for CO oxidation. *Catal. Commun.* **2006**, *7*, 281–284. [CrossRef]
40. Herzing, A.A.; Tang, Z.R.; Edwards, J.K.; Enache, D.I.; Bartley, J.K.; Taylor, S.H.; Carley, A.F.; Kiely, C.J.; Hutchings, G.J. Characterization of Au-based Catalysts Using Novel Cerium Oxide Supports. *Microsc. Microanal.* **2007**, *13*, 102–103. [CrossRef]

41. Venezia, A.M.; Pantaleo, G.; Longo, A.; Di Carlo, G.; Casaletto, M.P.; Liotta, F.L.; Deganello, G. Relationship between Structure and CO Oxidation Activity of Ceria-Supported Gold Catalysts. *J. Phys. Chem. B* **2005**, *109*, 2821–2827. [CrossRef]
42. Bera, P.; Hegd, M.S. Characterization and catalytic properties of combustion synthesized Au/CeO_2 catalyst. *Catal. Lett.* **2002**, *79*, 75. [CrossRef]
43. Liu, W.; Flytzani-Stephanopoulos, M.; Sarofim, A.F. *Selective Catalytic Reduction of Sulfur Dioxide to Elemental Sulfur*; Final Report; Office of Scientific and Technical Information (OSTI): Oak Ridge, TN, USA, 1995.
44. Haruta, M. Size- and support-dependency in the catalysis of gold. *Catal. Today* **1997**, *36*, 153–166. [CrossRef]
45. Yuan, Y.Z.; Asukura Wan, H.L.; Tsai, K.; Iwasawa, Y. Preparation of supported gold catalysts from gold complexes and their catalytic activities for CO oxidation. *Catal. Lett.* **1996**, *42*, 15–20. [CrossRef]
46. Mafune, F.; Kohno, J.; Takeda, Y.; Kondow, T. Formation of gold nanonetworks and small gold nanoparticles by irradiation of intense pulsed laser onto gold nanoparticles. *J. Phys. Chem. B* **2003**, *107*, 12589. [CrossRef]
47. Sims, C.M.; Maier, R.A.; Johnston-Peck, A.C.; Gorham, J.M.; Hackley, V.A.; Nelson, B.C. Approaches for the quantitative analysis of oxidation state in cerium oxide nanomaterials. *Nanotechnology* **2018**, *30*, 085703. [CrossRef] [PubMed]
48. Palmqvist, A.E.C.; Wirde, M.; Gelius, U.; Muhammed, M. Surfaces of doped nanophase cerium oxide catalysts. *Nanostruct. Mater.* **1999**, *11*, 995–1007. [CrossRef]
49. Bêche, E.; Charvin, P.; Perarnau, D.; Abanades, S.; Flamant, G. Ce 3d XPS investigation of cerium oxides and mixed cerium oxide (CexTiyOz). *Surf. Interface Anal.* **2008**, *40*, 264–267. [CrossRef]
50. Boccuzzi, F.; Chiorino, A.; Manzoli, M.; Andreeva, D.; Tabakova, T. FTIR study of the low-temperature water–gas shift reaction on Au/Fe_2O_3 and Au/TiO_2 catalysts. *J. Catal.* **1999**, *188*, 176–185. [CrossRef]
51. Swain, G.; Sultana, S.; Naik, B.; Parida, K. Coupling of Crumpled-Type Novel MoS(2) with CeO(2) Nanoparticles: A Noble-Metal-Free p-n Heterojunction Composite for Visible Light Photocatalytic H(2) Production. *ACS Omega* **2017**, *2*, 3745–3753. [CrossRef]
52. Fu, Q.; Kudriavtseva, S.; Saltsburg, H.; Flytzani-Stephanopoulos, M. Gold–ceria catalysts for low-temperature water-gas shift reaction. *Chem. Eng. J.* **2003**, *93*, 41–53. [CrossRef]
53. Wagner, F.E.; Galvagno, S.; Milone, C.; Visco, A.M.; Stievano, L.; Calogero, S. Mössbauer characterisation of gold/iron oxide catalysts. *J. Chem. Soc. Faraday Trans.* **1997**, *93*, 3404–3409. [CrossRef]
54. Khoudiakov, M.; Gupta, M.C.; Deevi, S. Au/Fe_2O_3 nanocatalysts for CO oxidation by a deposition-prcipitation technique. *Nanotechnology* **2004**, *15*, 987–990. [CrossRef]
55. Vernieres, J.; Steinhauer, S.; Zhao, J.; Grammatikopoulos, P.; Ferrando, R.; Nordlund, K.; Djurabekova, F.; Sowwan, M. Site-Specific Wetting of Iron Nanocubes by Gold Atoms in Gas-Phase Synthesis. *Adv. Sci.* **2019**, *6*, 1900447. [CrossRef] [PubMed]
56. Kruis, F.E.; Fissan, H.; Peled, A. Synthesis of nanoparticles in the gas phase for electronic, optical, and magnetic applications—A review. *J. Aerosol Sci.* **1998**, *29*, 511–535. [CrossRef]
57. Pithawalla, Y.B.; El-Shall, M.S.; Deevi, S.C.; Ström, V.; Rao, K.V. Synthesis of Magnetic Intermetallic FeAl Nanoparticles from a Non-Magnetic Bulk Alloy. *J. Phys. Chem. B* **2001**, *105*, 2085–2090. [CrossRef]
58. El-Shall, M.S.; Abdelsayed, V.; Pithawalla, Y.B.; Alsharaeh, E.; Deevi, S.C. Vapor Phase Growth and Assembly of Metallic, Intermetallic, Carbon, and Silicon Nanoparticle Filaments. *J. Phys. Chem. B* **2003**, *107*, 2882–2886. [CrossRef]
59. Li, S.; Germanenko, I.N.; El-Shall, M.S. Nanoparticles from the vapor phase: Synthesis and characterization of Si, Ge, MoO_3, and WO_3 nanocrystals. *J. Clust. Sci.* **1999**, *10*, 533–547. [CrossRef]
60. Iizuka, Y.; Tode, T.; Takao, T.; Yatsu, K.; Takeuchi, T.; Tsubota, S.; Haruta, M. A kinetic and adsorption study of CO oxidation over unsupported fine gold powder and over gold supported on titanium dioxide. *J. Catal.* **1999**, *187*, 50. [CrossRef]
61. Liang, R.; Hu, A.; Persic, J.; Zhou, Y.N. Palladium Nanoparticles Loaded on Carbon Modified TiO_2 Nanobelts for Enhanced Methanol Electrooxidation. *Nano Micro Lett.* **2013**, *5*, 202–212. [CrossRef]
62. Akita, T.; Tanaka, K.; Tsubota, S.; Haruta, M. Analytical High-Resolution TEM Study on Au/TiO_2 Catalysts. *MRS Proc.* **2011**, *589*, 253. [CrossRef]
63. Tada, K.; Koga, H.; Hayashi, A.; Kondo, Y.; Kawakami, T.; Yamanaka, S.; Okumura, M. Theoretical Clarification of the Coexistence of Cl Effects on Au/TiO_2: The Interaction between Au Clusters and the TiO_2 Surface, and the Aggregation of Au Clusters on the TiO_2 Surface. *Bull. Chem. Soc. Jpn.* **2017**, *90*, 506–519. [CrossRef]

64. Camellone, M.F.; Fabris, S. Reaction Mechanisms for the CO Oxidation on Au/CeO_2 Catalysts: Activity of Substitutional Au^{3+}/Au^{+} Cations and Deactivation of Supported Au^{+} Adatoms. *J. Am. Chem. Soc.* **2009**, *131*, 10473–10483. [CrossRef] [PubMed]
65. Tana; Wang, F.; Li, H.; Shen, W. Influence of Au particle size on Au/CeO_2 catalysts for CO oxidation. *Catal. Today* **2011**, *175*, 541–545. [CrossRef]
66. Kim, H.Y.; Henkelman, G. CO Oxidation at the Interface between Doped CeO_2 and Supported Au Nanoclusters. *J. Phys. Chem. Lett.* **2012**, *3*, 2194–2199. [CrossRef]
67. Zhou, Z.; Kooi, S. The Role of the Interface in CO Oxidation on Au/CeO_2 Multilayer Nanotowers. *Adv. Funct. Mater.* **2008**, *18*, 2801–2807. [CrossRef]